

Analysis of short subdiffusive time series: scatter of the time-averaged mean-squared displacement

This article has been downloaded from IOPscience. Please scroll down to see the full text article.

2010 J. Phys. A: Math. Theor. 43 252001

(<http://iopscience.iop.org/1751-8121/43/25/252001>)

View [the table of contents for this issue](#), or go to the [journal homepage](#) for more

Download details:

IP Address: 93.158.4.31

The article was downloaded on 02/06/2010 at 08:22

Please note that [terms and conditions apply](#).

FAST TRACK COMMUNICATION

Analysis of short subdiffusive time series: scatter of the time-averaged mean-squared displacement

Jae-Hyung Jeon and Ralf Metzler

Department of Physics, Technical University of Munich, James-Franck Straße, 85747 Garching, Germany

E-mail: jae-hyung.jeon@ph.tum.de and metz@ph.tum.de

Received 14 April 2010, in final form 13 May 2010

Published 1 June 2010

Online at stacks.iop.org/JPhysA/43/252001**Abstract**

We analyse the statistical behaviour of short time series in systems performing subdiffusion. Comparing the non-ergodic continuous time random walk model to the ergodic fractional Brownian motion, we demonstrate that the scatter between individual trajectories is not purely dominated by finite sample size effects but preserves some of the characteristics of the individual processes. In particular we show that the distribution of the time-averaged mean-squared displacements allows one to clearly distinguish between the two stochastic mechanisms even for a very short time series.

PACS numbers: 02.50.-r, 05.40.Fb, 05.10.Gg

(Some figures in this article are in colour only in the electronic version)

1. Introduction

Diffusion processes are conventionally described in terms of the ensemble-averaged mean-squared displacement

$$\langle x^2(t) \rangle = \int x^2 P(x, t) dx, \quad (1)$$

determined as the spatial average over the probability density function $P(x, t)$ to find the test particle at position x at time t .¹ In what follows we consider systems in which the time evolution of the mean-squared displacement (MSD) (1) is subdiffusive in the sense that we observe [1, 2]

$$\langle x^2(t) \rangle = \frac{2K_\alpha}{\Gamma(1 + \alpha)} t^\alpha, \quad (2)$$

¹ We confine our analysis to the one-dimensional case for simplicity.

with $0 < \alpha \leq 1$, where K_α of dimension $[K_\alpha] = \text{cm}^2 \text{s}^{-\alpha}$ is the anomalous diffusion constant. The limit $\alpha = 1$ corresponds to regular Brownian motion. To avoid errors in the ensemble average due to inhomogeneities between individual particles (differences in mass, surface structure, etc), relatively early the idea of single-particle trajectory analysis was brought forward [3]. From the time series $x(t)$ recorded in such setups one determines the time-averaged mean-squared displacement (TA MSD)

$$\overline{\delta^2(\Delta, T)} = \frac{1}{T - \Delta} \int_0^{T-\Delta} (x(t + \Delta) - x(t))^2 dt. \quad (3)$$

Here Δ is referred to as the lag time and T denotes the overall measurement time (length of the time series). In contrast to its ensemble-averaged analogue (1), the TA MSD (3) is a two-time quantity in the sense that the position difference entering expression (3) corresponds to two points of the time series $x(t)$ separated by the lag time Δ . This property gives rise to some interesting effects, as discussed below.

Single-particle trajectory analysis has indeed become one of the standard tools to probe the physical properties of complex liquids and/or structured environments through tracking the motion of a test particle. For instance, this technique reveals the subdiffusive behaviour of larger tracers in the crowded environment of living biological cells [4, 5], or in reconstituted crowding environments [6]. Similar subdiffusion was also observed on larger scales, for example in the motion of individual bacteria in a biofilm [7]. In many of these studies significant scatter of the amplitude of the TA MSD between different trajectories have been observed [5, 7].

Amplitude scatter between individual trajectories, as shown in figure 1, may have different origins: (1) Spatial inhomogeneities, i.e. the tracer particle is exposed to areas with significantly varying diffusivities; the sojourn times in respective areas will then impact on the behaviour of individual trajectories. (2) Dynamic properties of the process, i.e. the process naturally leads to variations of the time average, as shown for non-ergodic continuous time random walk (CTRW) subdiffusion [8, 9] (see below). (3) Finiteness of the recorded trajectories, i.e. the scatter is due to insufficient sampling in the sense that, given the total measurement time T , the time series become too short to be statistically significant. Here we focus on the latter effect. In particular, we will demonstrate that while scatter occurs due to finite sample sizes for different subdiffusion mechanisms, both ergodic and non-ergodic, even for short trajectories the *distribution* of the scatter remains characteristic for the different stochastic mechanisms. This finding may provide a powerful tool to pin down the stochastic mechanism underlying a given measured time series.

2. Stochastic processes and MSD

We briefly introduce two prominent stochastic models for subdiffusion, the continuous time random walk (CTRW) [10] and fractional Brownian motion (FBM) [11], and discuss their behaviour in terms of ensemble and time-averaged MSDs. Especially, we will comment on the scatter between individual trajectories in the long measurement time limit. In the next section we will then analyse their behaviour when the measurement time T becomes relatively short.

In a CTRW process each jump is characterized by a jump length and a waiting time with respect to the previous jump, both drawn independently from the corresponding waiting time and jump length distributions [10]. We here consider a process in which the jump lengths have a finite variance $\langle \delta x^2 \rangle$, while the waiting times are drawn from a density function with the power-law asymptotics $\psi(t) \simeq \tau^\alpha / t^{1+\alpha}$ with $0 < \alpha < 1$. In this case, the ensemble-averaged

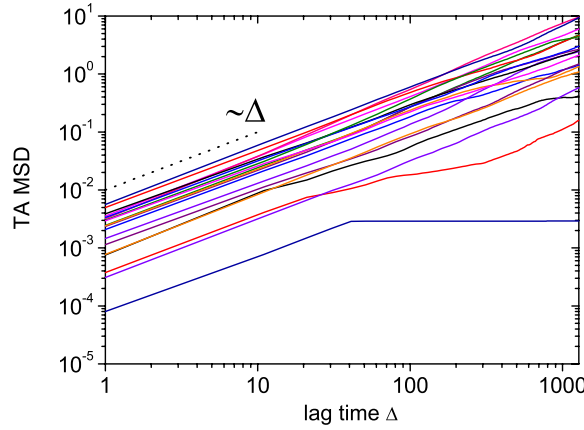


Figure 1. Time-averaged mean-squared displacement (TA MSD) for unconfined CTRW motion with $\alpha = 0.5$ and an overall trajectory length $T = 10^5$. We show 20 individual trajectories. In the lowest one, a single, extremely long waiting time event is causing a stalling of the trajectory. In other trajectories local changes of the slope are visible. Overall the amplitudes scatter considerably. The dotted line represents the expected linear slope according to equation (5).

MSD leads to the form (2). The divergence of the characteristic waiting time $\int_0^\infty t \psi(t) dt$ causes interesting effects such as ageing and weak ergodicity breaking [12, 13].

Indeed, in contrast to the ensemble-averaged MSD (2) the corresponding time-averaged quantity

$$\langle \overline{\delta^2(\Delta, T)} \rangle = \frac{1}{T - \Delta} \int_0^{T-\Delta} \langle (x(t + \Delta) - x(t))^2 \rangle dt \tag{4}$$

follows the scaling ($\Delta \ll T$) [8, 9]

$$\langle \overline{\delta^2(\Delta, T)} \rangle \sim \frac{2K_\alpha}{\Gamma(1 + \alpha)} \frac{\Delta}{T^{1-\alpha}}. \tag{5}$$

This lag-time dependence might deceivingly indicate normal diffusion. Only the overall measurement time T indicates the anomalous nature of the underlying process, in contrast to the ensemble average (2). The reason to use the additional ensemble average in relations (4) and (5) is that the pure time average $\overline{\delta^2(\Delta, T)}$ shows pronounced scatter around its ensemble average (4). This scatter is caused by the scale-free nature of CTRW subdiffusion: in the given time series there may occur a single or few events for which the individual waiting times become of the order of the measurement time T , no matter how long T is chosen (compare figure 1). In the derivation of expression (5) the additional ensemble averaging is thus necessary to include the average number of steps performed in the time interval Δ [9]. An example for the trajectory–trajectory scatter is shown in figure 1. Qualitatively this scatter is similar to the experimentally observed motion in [5]. The scatter is more pronounced at short T , see below. However, for CTRW subdiffusion processes even in the limit $T \rightarrow \infty$ the scatter remains present and reflects the inherent breaking of ergodicity. In fact, for sufficiently long trajectories the scatter follows the distribution [9]

$$\phi_\alpha(\xi) = \frac{\Gamma(1 + \alpha)^{1/\alpha}}{\alpha \xi^{1+1/\alpha}} l_\alpha \left(\frac{\Gamma(1 + \alpha)^{1/\alpha}}{\xi^{1/\alpha}} \right), \tag{6}$$

where $l_\alpha(z)$ is a one-sided Lévy stable distribution [14]² and we defined the dimensionless quantity $\xi = \overline{\delta^2} / \langle \delta^2 \rangle$. In the special case $\alpha = 1/2$ the distribution reduces to a Gaussian $\phi_{1/2}(\xi) = (2/\pi) \exp(-\xi^2/\pi)$, while in the Brownian limit $\alpha = 1$ ergodicity is restored, i.e. no scatter occurs: $\phi_1(\xi) = \delta(\xi - 1)$ [15]. We note that ergodicity is also broken in waiting time and jump length correlated random walk processes [16].

Under spatial confinement the TA MSD of CTRW subdiffusion shows a turnover from the law (5) to the power-law form $\langle \delta^2(\Delta, T) \rangle \simeq (\Delta/T)^{1-\alpha}$ [17, 18]. In an arbitrary confining potential $V(x)$ the behaviour is universal in the sense that the result [17]

$$\langle \delta^2(\Delta, T) \rangle \sim (\langle x^2 \rangle_B - \langle x \rangle_B^2) \frac{2 \sin(\pi\alpha)}{(1-\alpha)\pi\alpha} \left(\frac{\Delta}{T} \right)^{1-\alpha} \quad (7)$$

only depends on the first two moments of the corresponding Boltzmann distribution, $\langle x^n \rangle_B = \int x^n \exp(-\beta V(x)) dx / \int \exp(-\beta V(x)) dx$, where $\beta = 1/[k_B T]$ is the Boltzmann factor. This behaviour contrasts the plateau reached by the corresponding ensemble-averaged MSD. Only when the lag time Δ approaches the measurement time T , the TA MSD indeed jumps to the thermal value of the ensemble average.

In contrast to CTRW subdiffusion FBM is a Gaussian process with stationary increments. FBM may be described in terms of fractional Gaussian noise with zero mean and noise-noise correlation³

$$\langle \xi(t_1)\xi(t_2) \rangle = \alpha K_\alpha^*(\alpha - 1)|t_1 - t_2|^{\alpha-2} + 2\alpha K_\alpha^*|t_1 - t_2|^{\alpha-1}\delta(t_1 - t_2) \quad (8)$$

decaying as $\sim \alpha K_\alpha^*(\alpha - 1)|t_1 - t_2|^{\alpha-2}$. Here the dynamic exponent α is connected to the frequently used Hurst exponent H by $\alpha = 2H$. Specifically for subdiffusion we see that the noise is anticorrelated, i.e. a step in one direction is likely followed by a step in the opposite direction. The position coordinate of FBM then follows the law (1). Due to its stationary character FBM is ergodic [19], i.e. the TA MSD

$$\overline{\delta^2(\Delta, T)} = 2K_\alpha^*\Delta^\alpha, \quad (9)$$

is equivalent to the ensemble behaviour in the limit of long T . The same is true in a confined geometry where $\overline{\delta^2(\Delta, T)}$ reaches a plateau determined by the underlying interval size [20]. However, the approach to ergodicity in FBM is reached relatively slowly, in an algebraic fashion [19].

3. Single-particle trajectories and TA MSD in short trajectories

We now turn to the investigation of the scatter of the time average $\overline{\delta^2}$ for the two different subdiffusion processes. When dealing with the relatively short time series $x(t)$, we cannot invoke the above limiting theorems to derive the distribution ϕ . We therefore resort to a numerical analysis, supported by approximate limit distributions.

To this end a subdiffusive CTRW motion is generated from the density

$$\psi(t) = \frac{\alpha/\tau}{(1+t/\tau)^{1+\alpha}} \quad (10)$$

of waiting times, which asymptotically exhibits the required power-law scaling $\psi(t) \simeq \tau^\alpha/t^{1+\alpha}$. This form for $\psi(t)$ has the advantage that it converges for $t \rightarrow 0$ and is normalized. The jump lengths of this process are drawn from the Gaussian law $(2\pi)^{-1/2} \exp(-x^2/2)$. A

² The stable law $l_\alpha(t)$ is defined in terms of its characteristic function $\int_0^\infty l_\alpha(t) \exp(-ut) dt = \exp(-u^\alpha)$.

³ For consistency with typical FBM notation we use $K_\alpha^* \equiv K_\alpha / \Gamma(1 + \alpha)$.

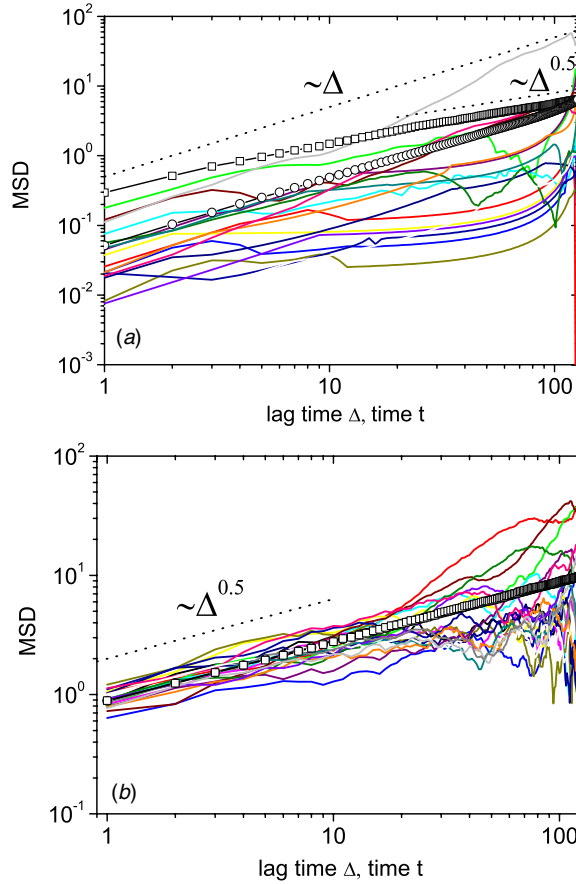


Figure 2. MSD for unconfined (a) CTRW and (b) FBM with $\alpha = 0.5$ and $T = 128$. Individual lines: twenty different time-averaged MSDs, $\overline{\delta^2(\Delta, T)}$. Open circle: ensemble-averaged TA MSD, $\langle \overline{\delta^2(\Delta, T)} \rangle$, from 10^4 realizations. Open square: ensemble-averaged MSD, $\langle x^2(t) \rangle$, from 10^4 realizations. Dotted line: expected scaling behaviours shown in equations (1), (5) and (9).

subdiffusive FBM was obtained by the recursive relation $x(t + \tau) = x(t) + \xi(t)$ (with $\tau = 1$) in terms of the fractional Gaussian noise $\xi(t)$, that was generated by the Hosking method [21]. In the case of confined motion, for both processes reflecting walls were placed at locations $x = \pm L$, such that during the simulations a particle jumping beyond the walls ($|x(t)| > L$) at some time t is bounced back to the position $x(t) - 2|x(t) - \text{sign}(x)L|$. For both cases, particle trajectories were simulated for an anomalous diffusion exponent $\alpha = 1/2$ and total number of time steps $T = 128$. It should be noted that such a seemingly small value for T is quite typical for many experimental realizations.

In figure 2 we show typical examples of TA MSDs for unconfined CTRW motion and FBM obtained from simulation. For comparison, we also include the ensemble-averaged quantities $\langle x^2(t) \rangle$ (open square) and $\langle \overline{\delta^2(\Delta, T)} \rangle$ (open circle) based on 10^4 realizations. First we note that the ensemble-averaged quantities follow the aforementioned scaling behaviours although the individual time series are short. For CTRW motion, $\langle \overline{\delta^2(\Delta, T)} \rangle$ differs from $\langle x^2(t) \rangle \simeq t^\alpha$ and grows linearly with Δ . For FBM, $\langle \overline{\delta^2} \rangle$ almost exactly coincides with $\langle x^2(t) \rangle \simeq t^\alpha$ when

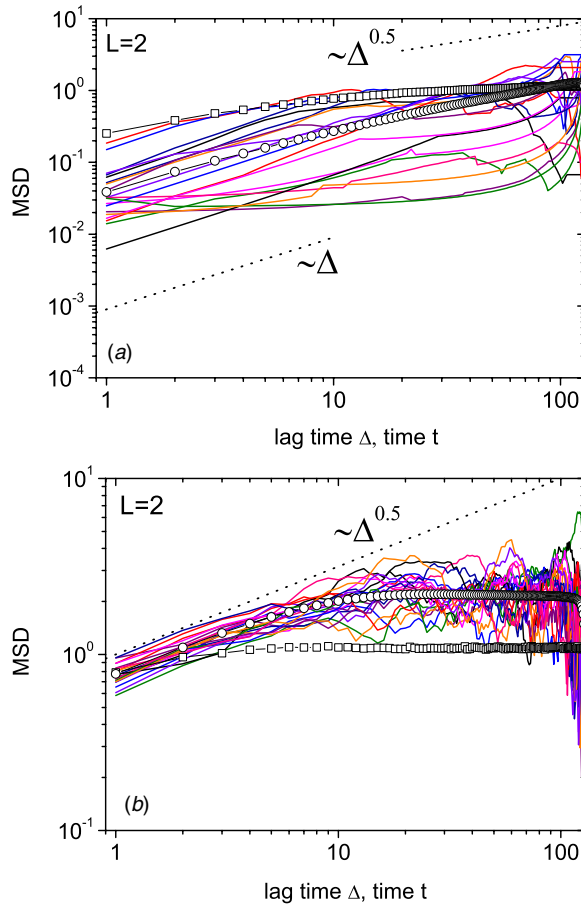


Figure 3. MSD for confined (a) CTRW and (b) FBM in an interval $[-L, L] = [-2, 2]$ with $\alpha = 0.5$ and $T = 128$. Individual lines: twenty different time-averaged MSDs, $\delta^2(\Delta, T)$. Open circle: ensemble-averaged TA MSD, $\langle \overline{\delta^2} \rangle$, from 10^4 realizations. Open square: ensemble-averaged MSD, $\langle x^2(t) \rangle$, from 10^4 realizations. Dotted line: expected scaling behaviours in free space.

Δ and t are being considered equivalent, due to the ergodic behaviour. On the other hand, individual TA MSDs from single trajectories, δ^2 , appear erratic and deviate from the expected scaling behaviours due to the insufficient averaging from the short time series. They exhibit considerable scatter in amplitude around the ensemble-averaged behaviour $\langle \overline{\delta^2} \rangle$.

Figure 3 depicts the results for confined motion. The ensemble-averaged second moments $\langle x^2(t) \rangle$ for both processes approximately reach the stationary value $\langle x^2 \rangle_{st} = L^2/3$ in the chosen interval $[-L, L]$. Similarly to the unbounded motion individual TA MSDs show erratic behaviour within individual trajectories as well as considerable trajectory–trajectory scatter due to insufficient time averaging. Especially for the CTRW case the curves do not converge to the saturation value because of its nonstationary characteristics. Given the noisy trajectories the motion could in fact be misinterpreted as a normal diffusive motion in free space. After averaging over several trajectories, however, the average curve $\langle \overline{\delta^2} \rangle$ can be clearly distinguished from normal Brownian motion because of the turnover in the scaling behaviours (i.e. from $\langle \overline{\delta^2}(\Delta, T) \rangle \simeq \Delta/T^{1-\alpha}$ to $\simeq (\Delta/T)^{1-\alpha}$), as demonstrated in equation (7). The

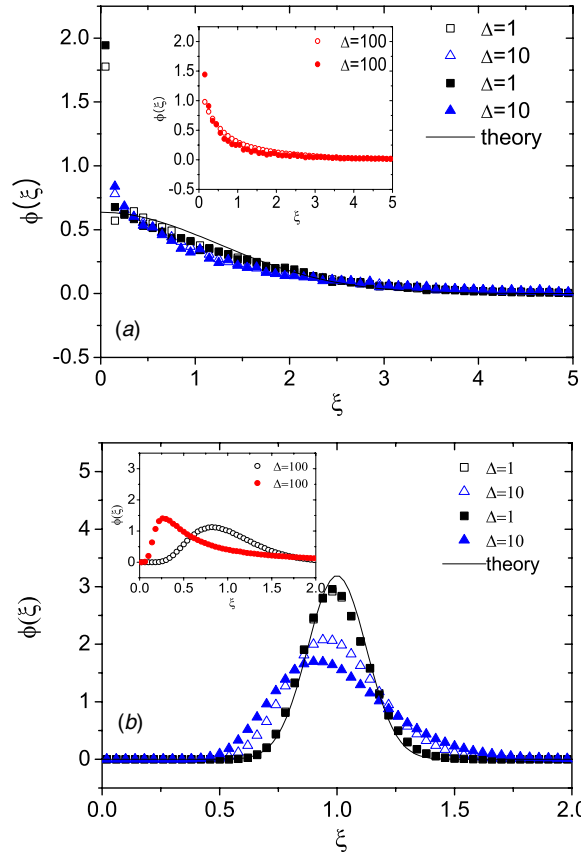


Figure 4. The distribution of TA MSDs, $\phi(\xi)$, with $\xi = \overline{\delta^2} / \langle \overline{\delta^2} \rangle$ for (a) CTRW motion and (b) FBM with $\alpha = 0.5$ and $T = 128$. The filled and open symbols, respectively, represent the cases for unconfined and confined motion. Shown in the insets are the distributions at $\Delta = 100$. Full lines in parts (a) and (b): limiting forms (6) and (11) for the corresponding distributions ϕ . Note the relatively small deviation from this limiting behaviour for the distributions obtained from our small samples.

CTRW subdiffusion amplitude scatter appears to be asymmetric around this averaged curve. In contrast, for the case of FBM, ergodicity ensures saturation in amplitude for individual TA MSDs as well as the average behaviour. However, as the time average stems from the short time series, $\langle \overline{\delta^2} \rangle$ does not fully converge to the ensemble-averaged second moment, $\langle x^2(t) \rangle$, which indicates that ergodicity is not fully satisfied. Different to the CTRW case, the scatter in the FBM trajectories appears symmetric around the centred average curve $\langle \overline{\delta^2} \rangle$. From this observation, we expect that the distribution of the TA MSDs may be clearly distinguishable between CTRW motion and FBM even for the short time series. In the next section we study the distribution in detail.

4. Distribution of TA MSDs

We obtained the normalized distributions $\phi(\xi)$ of the TA MSDs in terms of the dimensionless variable $\xi = \overline{\delta^2} / \langle \overline{\delta^2} \rangle$ from 10^6 realizations for each unconfined and confined stochastic motion with $T = 128$. Figure 4 shows the distributions with $\alpha = 0.5$ for both CTRW

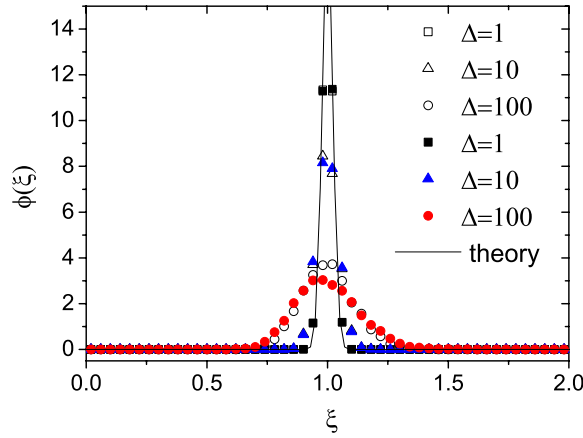


Figure 5. The distribution of TA MSDs, $\phi(\xi)$, for FBM with a longer time series having $T = 2^{12}$ and $\alpha = 0.5$. The closed and open symbols, respectively, represent the cases for unconfined and confined motion. The full line represents the theoretical behaviour (11) with $T = 2^{12}$ and $\Delta = 1$.

and FBM processes. The data clearly show that the distributions already possess distinct features originating from their inherent stochastic properties even for a time series as short as $T = 128$.

For the CTRW case, the distribution $\phi(\xi)$ monotonically decreases from the maximum at $\xi = 0$, which indicates the strong non-ergodicity of the motion. No significant dependence on the confinement and lag time are found in the distributions. In addition, they almost follow the analytical form (6) obtained in the assumption of the long time limit and without confinement, as shown in figure 4(a). This universal behaviour is due to the fact that the subdiffusive motion in CTRW arises from the scale-free waiting time distribution between successive jumps, not from the spatial property of successive jumps. Since individual trajectories are typically dominated by few long waiting time events, spatial confinement does not significantly change the distribution. By the same token, the distribution is almost insensitive to the total measurement time T , as seen in figure 4(a).

Differing from the CTRW case, the distributions for FBM are much more localized around their ensemble average $\langle \delta^2 \rangle$. It can be inferred that this property is related to the ergodicity of the motion, where a time-averaged observable from a single time series approaches the ensemble-averaged value as the measurement time T increases. Because of this property, the distribution for FBM is expected to depend on the measurement time T , its width decreasing with growing T . This is indeed confirmed in figure 5 where the distribution with a longer time series $T = 2^{12}$ is presented.

For FBM, the exact analytical form of the distribution has not been calculated. The long-ranged correlation between displacements $x(t + \Delta) - x(t)$ at different times for subdiffusive motion ($0 < \alpha < 1$) renders such a derivation difficult. However, it can be shown that the distribution approximately follows the Gaussian (see the appendix)

$$\phi(\xi) = \sqrt{\frac{T - \Delta}{4\pi\tau}} \exp\left(-\frac{(\xi - 1)^2(T - \Delta)}{4\tau}\right), \quad (11)$$

provided that the lag time Δ is short such that the time intervals between any two displacements $[x(t_i + \Delta) - x(t_i)]$ and $[x(t_j + \Delta) - x(t_j)]$ do not overlap for most displacements in $\overline{\delta^2}$ (i.e.

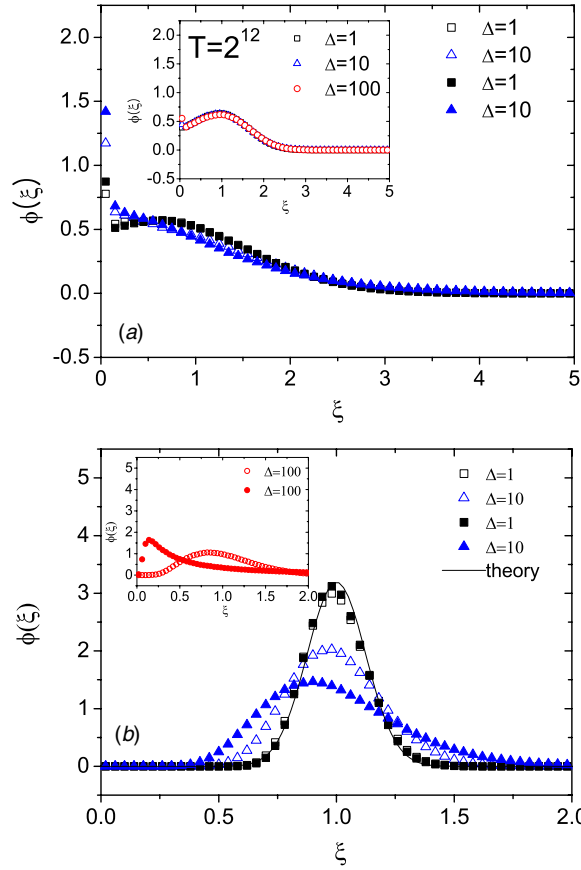


Figure 6. Distributions of TA MSDs for (a) CTRW and (b) FBMs with $\alpha = 0.75$, $T = 128$, and $L = 2$ (for confined motion). The filled and open symbols, respectively, represent the cases for unconfined and confined motion. The insets show the distributions at $\Delta = 100$. In the inset of part (a) a longer time series was used, created by a confined CTRW with $T = 2^{12}$. Full line in part (b): approximate Gaussian form (11) for the distribution ϕ .

$|t_i - t_j| > \Delta$). Under this condition, the two-point correlation function for the displacement is given by

$$\langle [x(t_i + \Delta) - x(t_i)][x(t_j + \Delta) - x(t_j)] \rangle \approx \alpha(\alpha - 1) K_\alpha^* \Delta^\alpha \left(\frac{\Delta}{|t_i - t_j|} \right)^{2-\alpha}, \quad (12)$$

which shows that displacements have very weak correlations for long time differences. Then, the displacements can be approximated as independent, which leads to the form (11). This is the case for $\Delta = 1$ in figures 4 and 5, where the theoretical lines for given T and Δ describe the distribution quite well. Note that the width of the distribution is inversely proportional to T in equation (11), such that in the limit of $T \rightarrow \infty$, $\phi(\xi)$ becomes a sharp peak of the form $\delta(\xi - 1)$, as expected from ergodicity. For longer lag times ($\Delta = 10$ and 100), we found that the simulated results do not follow the approximated form (11), as anticipated, since the correlations appear longer ranged in $\bar{\delta}^2$. The strong correlation tends to broaden the width. Here $\bar{\delta}^2$ can be viewed effectively as weakly correlated groups of displacements where each group comprises strongly correlated displacements. Since each group has roughly Δ

elements (in other words, $O(T/\Delta)$ groups in $\overline{\delta^2}$), this will lead to the observed broadening of the distribution $\phi(\xi)$.

The distributions are asymmetric for $\Delta = 10, 100$ in figure 4(b). Note that this is not related to the correlations of FBM trajectories but rather to the short measurement time T . The corresponding distributions with a longer time series in figure 5 are indeed symmetric. As seen in the disagreement between $\langle x^2 \rangle$ and $\langle \overline{\delta^2} \rangle$ in figure 3(b), this asymmetry in the distribution indicates that the motion is not fully ergodic within the given short measurement time.

To investigate the effect of the subdiffusion exponent α on the distribution, we obtained corresponding distributions for the value $\alpha = 0.75$, shown in figure 6. While the distributions for FBM are almost unchanged with respect to the theoretical behaviour (11), the ones for CTRW appear noticeably different. Now the peak is shifted to approximately $\xi = 1$ for the case of $\Delta = 1$, an effect that can be understood such that the non-ergodicity of the CTRW motion weakens as the given $\alpha = 0.75$ is closer to the limiting value $\alpha = 1$ at which the CTRW motion becomes ergodic. We found that the monotonic decrease in ϕ for $\Delta = 10$ and 100 (not shown) is due to the short length of the time series. As shown in the inset, the distributions with the longer time series $T = 2^{12}$ consistently have the expected limiting form, independent of the value of Δ .

5. Conclusions

We analysed the scatter of time-averaged mean-squared displacements for very short subdiffusive time series, that are characterized in terms of non-ergodic CTRW and ergodic FBM processes. We found that individual TA MSDs do not exhibit the scaling behaviour expected from the corresponding stochastic theory due to the rather short length of the time series. However, the associated distributions possess distinct features originating from intrinsic characteristics of the corresponding stochastic motions even for these short time series. We therefore expect that the distributions of the TA MSDs are a good measure to distinguish the two subdiffusive mechanisms in cases when long time series are not available. An important application is the analysis of subdiffusive motion of various biomolecules inside cells via single-particle tracking experiments where long time measurements are typically limited [22].

Acknowledgments

We acknowledge discussions with Stas Burov and Eli Barkai. This project was supported by the Deutsche Forschungsgemeinschaft.

Appendix

In this appendix we derive the analytical form of $\phi(\xi)$ for FBM under some assumptions described below. For a given trajectory $x(t)$, the TA MSD is written in a discrete form as

$$\overline{\delta^2(\Delta, T)} = \sum_i \tau \frac{[x(t_i + \Delta) - x(t_i)]^2}{T - \Delta} = \sum_i \tau \frac{Y_i}{T - \Delta} \quad (\text{A.1})$$

with the variable $Y_i = [x(t_i + \Delta) - x(t_i)]^2$, that is random but correlated for FBM. To characterize its correlation strength, we consider the correlation function between displacements $Y_i^{1/2}$ at different time steps

$$\langle Y_i^{1/2} Y_j^{1/2} \rangle = \langle [x(t_i + \Delta) - x(t_i)][x(t_j + \Delta) - x(t_j)] \rangle \quad (\text{A.2})$$

with the condition $t_i > t_j$ for convenience, without loss of generality. Using the relation ($t \geq s$)

$$\langle x(t)x(s) \rangle = K_\alpha^* [|t|^\alpha + |s|^\alpha - (t-s)^\alpha], \tag{A.3}$$

we can obtain the following expression for equation (A.2):

$$\langle Y_i^{1/2} Y_j^{1/2} \rangle = K_\alpha^* [(t_i + \Delta - t_j)^\alpha + |t_i - \Delta - t_j|^\alpha - 2(t_i - t_j)^\alpha]. \tag{A.4}$$

In the case when the time difference is larger than the lag time (i.e. $t_i - t_j > \Delta$), the correlation function can be approximated by

$$\begin{aligned} & K_\alpha^* [(t_i - t_j + \Delta)^\alpha + (t_i - t_j - \Delta)^\alpha - 2(t_i - t_j)^\alpha], \\ & = K_\alpha^* (t_i - t_j)^\alpha \left[\left(1 + \frac{\Delta}{t_i - t_j}\right)^\alpha + \left(1 - \frac{\Delta}{t_i - t_j}\right)^\alpha - 2 \right], \end{aligned} \tag{A.5}$$

$$\approx \alpha(\alpha - 1) K_\alpha^* \Delta^\alpha \left(\frac{\Delta}{t_i - t_j} \right)^{2-\alpha}. \tag{A.6}$$

Thus, the correlation is weak between displacements for large time differences compared to the lag time. As a special case for $\alpha = 1$, no correlation exists for non-overlapping time intervals. In the opposite case when the time difference is smaller than the lag time (i.e. $t_i - t_j < \Delta$), the correlation function can have non-negligible values, even at $\alpha = 1$,

$$\langle Y_i^{1/2} Y_j^{1/2} \rangle = K_\alpha^* [(1 + \gamma)^\alpha + (1 - \gamma)^\alpha - 2\gamma^\alpha] \Delta^\alpha \tag{A.7}$$

where γ is a value ranging from 0 to 1 satisfying $t_i - t_j = \gamma \Delta$.

The analysis indicates that the TA MSD is evaluated from a larger range of correlated displacements as Δ increases. For $\Delta = 1$, nearly all Y_i are weakly coupled (since they are the displacements of non-overlapping time intervals) and thus, for $T \gg 1$, $\delta^2(\Delta = 1, T)$ can be obtained from the approximation that the Y_i are statistically independent.

We now obtain the distribution $\phi(\xi)$ under this assumption. Its characteristic function $G_\xi(k)$ can be constructed as follows:

$$G_\xi(k) = \int d\xi e^{ik\xi} \phi(\xi) = \langle e^{ik\xi} \rangle \tag{A.8}$$

$$= \left\langle \exp \left(ik \sum_j \frac{\tau Y_j}{(T - \Delta) \langle \delta^2 \rangle} \right) \right\rangle \tag{A.9}$$

$$= \exp \left(\sum_j \ln \left\langle \exp \left(i \frac{k\tau}{(T - \Delta) \langle \delta^2 \rangle} Y_j \right) \right\rangle \right) \tag{A.10}$$

where the last expression follows from the statistical independence of Y_j . Using $G_j = \langle \exp \left(i \frac{k\tau}{(T - \Delta) \langle \delta^2 \rangle} Y_j \right) \rangle$, the logarithm of the characteristic function is expanded as

$$\ln G_j = ik\tau \frac{\langle Y_j \rangle}{(T - \Delta) \langle \delta^2 \rangle} - \frac{k^2 \tau^2 [\langle Y_j^2 \rangle - \langle Y_j \rangle^2]}{2(T - \Delta)^2 \langle \delta^2 \rangle} \tag{A.11}$$

for $T \gg 1$. For free FBM, from the relation $\langle \delta^2 \rangle = \langle Y_j \rangle = 2K_\alpha^* \Delta^\alpha$ and $\langle Y_j^2 \rangle = 4(K_\alpha^*)^2 \Delta^{2\alpha}$, we find the characteristic function

$$G_\xi(k) = \exp \left(\sum_j \ln \left\langle \exp \left(i \frac{k\tau}{(T - \Delta) \langle \delta^2 \rangle} Y_j \right) \right\rangle \right) \approx e^{ik - k^2 \tau / (T - \Delta)} \tag{A.12}$$

By Fourier inversion we finally obtain the distribution function of the MSD,

$$\phi(\xi) = \sqrt{\frac{T - \Delta}{4\pi\tau}} \exp\left(-\frac{(\xi - 1)^2(T - \Delta)}{4\tau}\right). \quad (\text{A.13})$$

References

- [1] Bouchaud J-P and Georges A 1990 *Phys. Rep.* **195** 127
- [2] Metzler R and Klafter J 2000 *Phys. Rep.* **339** 1
- [3] Nordlund I 1914 *Z. f. Phys. Chem.* **87** 40–62
- [4] Seisenberger G, Ried M U, Endreß T, Büning H, Hallek C M and Bräuchle 2001 *Science* **294** 1929
Gal N and Wehls D 2010 *Phys. Rev. E* **81** 020903(R)
- [5] Bronstein I, Israel Y, Kepten E, Mai S, Shav-Tal Y, Barkai E and Garini Y 2009 *Phys. Rev. Lett.* **103** 018102
Golding I and Cox E C 2006 *Phys. Rev. Lett.* **99** 098102
Tolić-Nørrelykke I M, Munteanu E L, Thon G, Oddershede L and Berg-Sørensen K 2004 *Phys. Rev. Lett.* **93** 078102
Caspi A, Granek R and Elbaum M 2002 *Phys. Rev. E* **66** 011916
- [6] Wong I Y, Gardel M L, Reichman D R, Weeks E R, Valentine M T, Bausch A R and Weitz D A 2004 *Phys. Rev. Lett.* **92** 178101
Pan W, Filobelo L, Pham N D Q, Galkin O, Uzunova V V and Vekilov P G 2009 *Phys. Rev. Lett.* **102** 058101
- [7] Rogers S S, van der Walle C and Waigh T A 2008 *Langmuir* **24** 13549
- [8] Lubelski A, Sokolov I M and Klafter J 2008 *Phys. Rev. Lett.* **100** 250602
- [9] He Y, Burov S, Metzler R and Barkai E 2008 *Phys. Rev. Lett.* **101** 058101
- [10] Scher H and Montroll E W 1975 *Phys. Rev. B* **12** 2455
Klafter J, Blumen A and Shlesinger M F 1987 *Phys. Rev. A* **35** 3081
- [11] Kolmogorov A N 1940 *Dokl. Acad. Sci. USSR* **26** 115
Mandelbrot B B and van Ness J W 1968 *SIAM Rev.* **1** 422
- [12] Monthus C and Bouchaud J-P 1996 *J. Phys. A: Math. Gen.* **29** 3847
Barkai E and Cheng Y C 2003 *J. Chem. Phys.* **118** 6167
- [13] Bouchaud J-P 1992 *J. Phys. I* **2** 1705
Bel G and Barkai E 2005 *Phys. Rev. Lett.* **94** 240602
Rebenshtok A and Barkai E 2007 *Phys. Rev. Lett.* **99** 210601
Lomholt M A, Zaid I M and Metzler R 2007 *Phys. Rev. Lett.* **98** 200603
- [14] Hughes B D 1995 *Random Walks and Random Environments (Random Walks vol 1)* (Oxford: Oxford University Press)
- [15] Metzler R, Tejedor V, Jeon J-H, He Y, Deng W H, Burov S and Barkai E 2009 *Acta Phys. Pol. B* **40** 1315
- [16] Tejedor V and Metzler R 2010 *J. Phys. A: Math. Theor.* **43** 082002
- [17] Burov S, Metzler R and Barkai E 2010 arXiv:1003.3182
- [18] Neusius T, Sokolov I M and Smith J C 2009 *Phys. Rev. E* **80** 011109
- [19] Deng W H and Barkai E 2009 *Phys. Rev. E* **79** 011112
- [20] Jeon J-H and Metzler R 2009 *Phys. Rev. E* **81** 021103
- [21] Hosking J R M 1984 *Water Resour. Res.* **20** 1898
- [22] Tejedor V, Bénichou O, Voituriez R, Jungmann R, Simmel F, Selhuber C, Oddershede L and Metzler R 2010 *Biophys. J.* **98** 1364